OSTI ID: 1280374

Ubiquitous signatures of nematic quantum criticality in optimally doped Fe-based superconductors

Hsueh-Hui Kuo[1,2,*], Jiun-Haw Chu[1,3,*†], Johanna C. Palmstrom[1,3], Steven A. Kivelson[1,4], Ian R. Fisher[1,3,†]

[1]Stanford Institute of Energy and Materials Science,SLAC National Accelerator Laboratory, 2575 Sand Hill Road, Menlo Park 94025,California 94305, USA,

[2]Department of Material Science and Engineering and Geballe Laboratory for Advanced Materials, Stanford University, Stanford, California 94305, USA,

[3]Department of Applied Physics and Geballe Laboratory for Advanced Materials, Stanford University, Stanford, California 94305, USA,

[4]Department of Physics and Geballe Laboratory for Advanced Materials, Stanford University, Stanford, California 94305, USA,

[†]To whom correspondence should be addressed;
E-mail:arrowchu@gmail.edu(J.H.C.) irfisher@stanford.edu(I.R.F.)

[*]These authors contributed equally to this work

A key actor in the conventional theory of superconductivity is the induced interaction between electrons mediated by the exchange of virtual collective fluctuations, originally phonons. Other collective modes that can play the same role, especially spin-fluctuations, have been widely discussed in the context of high-temperature and heavy Fermion superconductors. The strength of such collective fluctuations is measured by the associated susceptibility. Here we use differential elastoresistance measurements on five optimally doped Fe-based superconductors to reveal that a diverging *nematic* susceptibility appears to be a generic feature in the optimal doping regime of these materials. The observation motivates consideration of the effects of nematic fluctuations on the

This material is based upon work supported by the U.S. Department of Energy, Office of Science, Office of Basic Energy Sciences, Division of Materials Sciences and Engineering, under Contract No. DE-AC02-76SF00515.

superconducting pairing interaction in this family of compounds, and possibly beyond.

A growing body of evidence suggests the possibility of an intimate connection between electronic nematic phases (*1*) and high-temperature superconductivity. However, it is currently unclear to what extent there is any causal relationship between nematic fluctuations and superconductivity. Strongly anisotropic electronic phases have been found in the underdoped regime of both cuprate (*2, 3, 4, 5, 6*) and Fe-based (*7, 8, 9, 10, 11, 12*) high-temperature superconductors. For underdoped Fe-based systems, recent measurements of the elastoresisistance (*13, 14, 15*), Raman spectroscopy (*16, 17, 18*), and elastic moduli (*19, 20*) for the representative electron-doped system $Ba(Fe_{1-x}Co_x)_2As_2$ reveal a divergence of the electronic nematic susceptibility upon approach to the tetragonal-to-orthorhombic structural phase transition, definitively establishing that the phase transition is driven by electronic correlation. For the cuprates, recent x-ray diffraction (*21, 22, 23, 24*) and NMR (*25*) measurements have revealed evidence for short-range charge density wave order in "underdoped" crystals. Although details of the charge ordered state(s) are still being established, these initial observations have at least motivated discussion of a possible "vestigial" nematic order (*26*). Perhaps significantly, in the phase diagrams of both families of compounds, optimal doping is located close to putative quantum critical points (*27, 28, 29*) which potentially have a nematic character (*13, 26, 30*).

From a theoretical perspective, recent treatments indicate that nematic quantum criticality, (i.e. quantum critical fluctuations caused by proximity to a nematic quantum critical point) can provide an enhancement of the existing pairing interaction. In particular, a pure nematic phase does not break the translational symmetry of the original crystal lattice; consequently the q=0 nematic fluctuations enhance T_c in all symmetry channels (*31, 32, 33*). It is therefore of considerable interest to empirically establish whether nematic fluctuations are a characteristic feature of optimally doped high temperature superconductors, as well as to probe

the extent to which these nematic fluctuations show intrinsically quantum behavior. In the present paper, we show that this is the case for Fe-pnictide and chalcogenide superconductors by considering the representative materials $Ba(Fe_{1-x}Co_x)_2As_2$ and $Ba(Fe_{1-x}Ni_x)_2As_2$ (i.e. electron-doped "122"), $Ba_{1-x}K_xFe_2As_2$ (hole-doped), $BaFe_2(As_{1-x}P_x)_2$ (isovalent substitution) and $FeTe_{1-x}Se_x$ ("11"). Furthermore, we find that the nematic susceptibility obeys a simple Curie-Weiss power law for all five optimally doped Fe-based superconductors over a wide temperature range. For the electron and hole-doped 122 pnictides a sub-Curie-Weiss deviation was observed at low temperatures, which we tentatively attribute to an enhanced sensitivity to disorder in a quantum critical regime.

Nematic order couples linearly to anisotropic strain of the same symmetry. Consequently, the nematic susceptibility of a material can be measured by considering the electronic anisotropy that is induced by anisotropic in-plane strain. In the regime of infinitesimal strains, all forms of electronic anisotropy are linearly proportional. Hence, the rate of change of resistivity anisotropy with respect to anisotropic strain, defined in the limit of vanishing strain, is linearly proportional to the nematic susceptibility (*34*). The proportionality constant depends on microscopic physics, but away from any quantum critical point does not contain any singular behavior. Consequently, the induced resistivity anisotropy reveals the essential divergence of the nematic susceptibility upon approach to a thermally-driven nematic phase transition (*14,15*).

For a tetragonal material, nematic order has either d_{xy} symmetry (i.e. the B_{2g} irreducible representation of the D_{4h} point group, corresponding to nematic order oriented along a nearest-neighbor Fe-Fe bond – the [110] or [1$\bar{1}$0] crystal axes), or $d_{x^2-y^2}$ symmetry (B_{1g}, corresponding to the [100] or [010] crystal axes). Anisotropic strains with appropriate symmetry are then $\epsilon_6 = (\epsilon_{xy}+\epsilon_{yx})/2$ and $\epsilon_1 - \epsilon_2 = \epsilon_{xx} - \epsilon_{yy}$ respectively. The strain-induced changes in resistivity can be described using the dimensionless elastoresistivity tensor, m_{ij} (*14*):

$$(\Delta\rho/\rho)_i = \sum_{j=1}^{6} m_{ij}\epsilon_j \tag{1}$$

where $1 = xx$, $2 = yy$ etc. Consequently, the corresponding components of the nematic susceptibility tensor are given by:

$$\chi_{N(B_{2g})} = c \times 2m_{66} \tag{2}$$

$$\chi_{N(B_{1g})} = c' \times (m_{11} - m_{12}) \tag{3}$$

where c and c' are proportionality constants, which depend on microscopic physics (*34*).

We measure elastoresistivity by applying an in-situ tunable anisotropic strain using a piezoelectric PZT stack. A square plate sample (typical dimension 750x750x20 μm) is glued on the side wall of the PZT stack using a commercial two part epoxy. The PZT stack deforms when a voltage is applied and hence strains the sample glued on top of it (*35*). The amount of strain can be measured by a strain gauge glued either on the backside of the PZT stack or on the top surface of a larger sample(the latter case enabling a full determination of the strain transmission (*36*)). The in-plane resistivity tensor of the sample is measured via the Montgomery technique, with electrical contacts made at the four corners of the square sample (*36*). Representative data taken using this new technique are shown in Figure 1 for the specific case of $BaFe_2As_2$. As has been previously demonstrated (*14, 15*), the data can be fit very well by a Curie-Weiss temperature dependence:

$$2m_{66} = 2m_{66}^0 + \lambda/[a(T - T^*)]. \tag{4}$$

In Figure 2 we show B_{2g} elastoresistance data for a range of optimally doped materials, including $BaFe_2(As_{1-x}P_x)_2$ (isovalently substituted), $Ba(Fe_{1-x}Ni_x)_2As_2$ (electron-doped),

$Ba_{1-x}K_xFe_2As_2$ (hole-doped) and $FeTe_{1-x}Se_x$. In all cases, $2m_{66}$ rises strongly with decreasing temperature, with comparably large values for each compound. The observation of such an effect for this wide variety of ways of doping, including the case of the iron chalcogenide $FeTe_{0.6}Se_{0.4}$, is highly suggestive that a divergence of the nematic susceptibility in the B_{2g} channel is a generic feature of optimally doped Fe-based superconductors. This is our main result. Regardless of microscopic models, from a purely empirical perspective it is apparent that the optimally-doped superconductor is born out of an electronic state that is characterized by strongly fluctuating orientational (nematic) order in this specific symmetry channel. This result is especially notable for $FeTe_{0.6}Se_{0.4}$ given that the orientation of both the magnetic ordering wave vector and the in-plane component of the structural distortion of undoped FeTe is 45 degrees away from the orientation of those in the iron arsenide materials.

The m_{66} coefficient of optimally doped $BaFe_2(As_{0.68}P_{0.32})_2$ (Fig. 2A) follows a perfect Curie-Weiss temperature dependence from $T = 250K$ (the highest temperature where strain can be effectively transmitted by the epoxy) down to T_c (below which temperature the resistance is zero), with a Weiss temperature (T^*) close to zero. For $FeTe_{0.6}Se_{0.4}$, the m_{66} coefficient can be perfectly fitted with Cure-Weiss down to T_c but shows a significant deviation for temperatures greater than 100K, possibly related to the loss of quasi particle coherence due to its extremely small Fermi energy as observed in photoemission spectroscopy and transport (*37,38*). Intriguingly, for the electron and hole doped 122 pnictides, a downward deviation from Curie-Weiss behavior is observed below a characteristic temperature that is different for each of the materials. The quality of fit to the Curie-Weiss functional form for $BaFe_2(As_{0.68}P_{0.32})_2$ in comparison to all of the other optimally doped compositions studied can be readily appreciated if the data are plotted on log axes (Fig. S11). Only the data for the P-substituted system can be fit by a single power law [$|(2m_{66} - 2m_{66}^0)| \sim (T - T^*)^{-\gamma}$] over the entire temperature range, yielding $\gamma = 0.985 \pm 0.005$ and $T^* = 11.7 \pm 3.1$.

A slightly overdoped $BaFe_2(As_{0.64}P_{0.36})_2$ sample has also been measured; the elastoresistivity coefficient m_{66} of this sample can also be well fitted by Curie-Weiss temperature dependence over the entire temperature range, with a negative Weiss temperature $T^* = -11.5 \pm 2.3$(Fig. S14). The small value of the Weiss temperature observed in $BaFe_2(As_{1-x}P_x)_2$ near optimally doping, and the fact that it crosses zero as doping increases, motivates consideration of the nematic susceptibility in the context of a quantum critical point. An Ising nematic phase transition in an insulator would generally be expected to have dynamical exponent $z = 1$, so the effective dimensionality of the system would be $d + z$ = 3+1. As the materials in question are metallic, the situation is more complicated (*39*); the Hertz-Millis paradigm is expected to break down in the case of electronic nematic order in metallic systems, for which Landau damping associated with the gapless Fermions leads to a larger value of the dynamical exponent, z = 3. Although the analysis of this problem is not straightforward, both analytic (*40*) and numerical studies (*41*) indicate that the nematic susceptibility at criticality should diverge in proportion to 1/T (up to possible logarithmic corrections), consistent with the observed behavior of the B_{2g} elastoresistance of optimally doped $BaFe_2(As_{1-x}P_x)_2$.

To gain insight into the physical origin of the low temperature downward deviation from Curie-Weiss behavior in the electron and hole doped pnictides, we consider the evolution of the B_{2g} elastoresistance as a function of composition for the specific case of Co-doped $BaFe_2As_2$. Figure 3 A-D show the progression of $2m_{66}$ as a function of Co doping for several representative compositions (more were measured, see (*36*)), from underdoped (A,B), through optimal doping (C), to the overdoped regime (D). For the heavily underdoped compositions(x = 0.025), $2m_{66}$ can be well described by mean field Curie-Weiss T-dependence down to T_s. It has been previously established that this behavior is essentially independent of disorder, at least comparing undoped $BaFe_2As_2$ with different Residual Resistance Ratios (RRR), and Co and Ni substituted crystals with the same T_N (*15*). The Weiss temperature T^* extracted from high-

temperature fits to Curie-Weiss behavior crosses zero close to optimal doping (Fig. 4). However, for lightly underdoped $Ba(Fe_{0.553}Co_{0.047})_2As_2$, a downward deviation from mean-field behavior at low temperatures begins to be noticeable, and becomes more pronounced for optimally doped $Ba(Fe_{0.93}Co_{0.07})_2As_2$; similar deviations are observed in optimally Ni and K doped $BaFe_2As_2$. A similar effect has been observed in recent measurements of the sheer modulus via three-point bending experiments (*20*). The deviation from Curie-Weiss behavior diminishes again as the doping is further increased: for the overdoped composition (Fig. 3D) the data can be fit to Curie-Weiss to a lower temperature than for optimal doping, and the magnitude of the deviation below ~ 45 K is smaller than for optimal doping. $2m_{66}$ of four additional Co dopings has also been measured, showing a similar non-monotonic doping dependence of the deviation from Curie-Weiss behavior. The fact that the effect is maximal near optimal doping where $T^* \sim 0$, suggests that it is associated with proximity to the putative nematic quantum phase transition.

P-substituted $BaFe_2As_2$ is the "cleanest" of all of the known 122 Fe-pnictide families, evidenced by the fact that quantum oscillations can be observed across the phase diagram (*42, 43*). The deviation from Curie-Weiss behavior for optimally doped compositions of all other dopants in $BaFe_2As_2$ suggests that disorder plays an important role in the quantum critical regime. All forms of quenched disorder produce locally anisotropic effective strains, which thus couple to the orientation of the nematic order; this is "random-field" disorder (*26*). Analysis of the random-field Ising model yields several generically expected effects of random field disorder, including suppression of the nematic susceptibility below mean field expectations for a clean system, and, for the case of a quantum phase transition, the enhanced sensitivity of quantum critical phenomena to disorder. (*36*).

The temperature dependence of the nematic susceptibility can also be extracted from measurements of the elastic moduli (*20*). The two measurements (elastoresistance and elastic moduli) are in broad agreement, for example in terms of the Curie-Weiss T-dependence of χ_N for

underdoped compositions of $Ba(Fe_{1-x}Co_x)_2As_2$, and also in terms of the deviation from Curie-Weiss behavior near optimal doping. However, there is an important distinction in terms of the relative magnitude of the measured quantities as a function of doping. In particular, the normalized lattice softening $[c_{66}^0 - c_{66}]/c_{66}^0$ extracted in (*20*) monotonically decreases in magnitude and extent in temperature as a function of x. In contrast, the quantity $|(2m_{66} - 2m_{66}^0)| = c\chi_N$ initially increases with x, peaking for lightly underdoped compositions $x \simeq 0.05$. The apparent enhancement of the elastoresistance $2m_{66}$ over the softening of the elastic modulus for compositions near optimal doping is potentially related to renormalization of the quasiparticle effective mass in the quantum critical regime, as has been seen in P-substituted $BaFe_2As_2$ (*29*). Such a mass renormalization is an expected consequence of nematic quantum critical fluctuations (*39*). Significantly, it is precisely these low-energy quasiparticles that are also involved in the eventual superconductivity.

References and Notes

1. E. Fradkin, S. A. Kivelson, M. J. Lawler, J. P. Eisenstein, A. P. Mackenzie, Nematic Fermi fluids in condensed matter physics. *Annu. Rev. Condens. Matter Phys.* **1**, 153-178 (2010).

2. Y. Ando, K. Segawa, S. Komiya, A. N. Lavrov, Electrical resistivity anisotropy from self-organized one dimensionality in high-temperature superconductors. *Phys. Rev. Lett.* **88**, 137005 (2002).

3. C. Howald, H. Eisaki, N. Kaneko, M. Greven, A. Kapitulnik, Periodic density-of-states modulations in superconducting $Bi_2Sr_2CaCu_2O_{8+}$. *Phys. Rev. B* **67**, 014533 (2003).

4. V. Hinkov *et al.*, Electronic liquid crystal state in the high-temperature superconductor $YBa_2Cu_3O_{6.45}$. *Science* **319**, 597 (2008).

5. R. Daou*et al.*, Broken rotational symmetry in the pseudogap phase of a high-T_C superconductor. *Nature* **463**, 519 (2010).

6. S. A. Kivelson *et al.*, How to detect fluctuating stripes in the high-temperature superconductors. *Rev. Mod. Phys.* **75**, 1201 (2003).

7. T. Chuang *et al.*, Nematic Electronic Structure in the "Parent" State of the Iron-Based Superconductor $Ca(Fe_{1x}Co_x)_2As_2$ *Science* **327**, 181 (2010)

8. Jiun-Haw Chu *et al.*, In-Plane Resistivity Anisotropy in an Underdoped Iron Arsenide Superconductor, *Science* **329**, 824 (2010).

9. M. A. Tanatar, *et. al.*, Uniaxial-strain mechanical detwinning of $CaFe_2As_2$ and $BaFe_2As_2$ crystals: Optical and transport study, *Phys. Rev. B* **81**, 184508 (2010)

10. A. Dusza, A. Lucarelli, F. Pfuner, J.-H. Chu, I. R. Fisher ,L. Degiorgi, Anisotropic charge dynamics in detwinned Ba(Fe1-xCox)2As2, *Euro. Phys. Letters* **93**, 37002 (2011)

11. Ming Yi *et al.*, Symmetry breaking orbital anisotropy observed for detwinned $Ba(Fe_{1-x}Co_x)_2As_2$ above the spin density wave transition, *Proc. Natl Acad. Sci. USA* **108** 6878-6883 (2011)

12. Xingye Lu *et al.*, Nematic spin correlations in the tetragonal state of uniaxial-strained $Ba(Fe_{1-x}Ni_x)_2As_2$, *Science* **345**, 657 (2014)

13. J.-H. Chu, H.-H. Kuo, J. G. Analytis, I. R. Fisher, Divergent Nematic Susceptibility in an Iron Arsenide Superconductor. *Science* **337**, 710-712 (2012).

14. H.-H Kuo, Maxwell C. Shapiro, Scott C. Riggs, Ian R. Fisher, Measurement of the elastoresistivity coefficients of the underdoped iron arsenide $Ba(Fe_{0.975}Co_{0.025})_2As_2$. *Phys. Rev. B* **88**, 085113 (2013).

15. H.-H Kuo, I. R. Fisher, Effect of Disorder on the Resistivity Anisotropy Near the Electronic Nematic Phase Transition in Pure and Electron-Doped $BaFe_2As_2$. *Phys. Rev. Lett.* **112**, 227001 (2014).

16. Y. Gallais *et. al.*, Observation of Incipient Charge Nematicity in $Ba(Fe_{1x}Co_x)_2As_2$. *Phys. Rev. Lett.* **111**, 267001 (2013).

17. V. K. Thorsmlle *et. al.*, Critical quadrupole fluctuations and collective modes in iron pnictide superconductors. *Phys. Rev. B* **93**, 054515 (2016).

18. F. Kretzschmar, *et al.*, Critical spin fluctuations and the origin of nematic order in $Ba(Fe_{1x}Co_x)_2As_2$. *Nat. Phys.* doi:10.1038/nphys3634 (2016).

19. M. Yoshizawa *et al.*, Structural quantum criticality and superconductivity in iron-based superconductor $Ba(Fe_{1x}Co_x)_2As_2$. *J. Phys. Soc. Jpn.* **81**, 024604 (2012).

20. A. E. Böhmer *et. al.*, Nematic Susceptibility of Hole-Doped and Electron-Doped $BaFe_2As_2$ Iron-Based Superconductors from Shear Modulus Measurements. *Phys. Rev. Lett.* **112**, 047001 (2014).

21. J. Chang *et al.*, Direct observation of competition between superconductivity and charge density wave order in $YBa_2Cu_3O_{6.67}$. *Nat. Phys.* **8**, 871 (2012).

22. G. Ghiringhelli *et al.*, Long-Range Incommensurate Charge Fluctuations in (Y,Nd)$Ba_2Cu_3O_{6+x}$. *Science* **337**, 821 (2012).

23. E. Blackburn *et al.* X-Ray Diffraction Observations of a Charge-Density-Wave Order in Superconducting Ortho-II $YBa_2Cu_3O_{6.54}$ Single Crystals in Zero Magnetic Field. *Phys. Rev. Lett.* **110**, 137004 (2013).

24. J. M. Tranquada, B. J. Sternlieb, J. D. Axe, Y. Nakamura, S. Uchida, Evidence for stripe correlations of spins and holes in copper oxide superconductors. *Nature* **375**, 561 (1995).

25. T. Wu, H. Mayaffre *et al.*, Magnetic-field-induced charge-stripe order in the high-temperature superconductor $YBa_2Cu_3O_y$. *Nature* **477**, 191 (2011).

26. L. Nie, G. Tarjus, S. A. Kivelson, Quenched disorder and vestigial nematicity in the pseudogap regime of the cuprates. *Proc. Natl. Acad. Sci. U.S.A.* **111**, 7980 (2014).

27. S. A. Kivelson, E. Fradkin, V. J. Emery, Electronic liquid-crystal phases of a doped Mott insulator. *Nature* **393**, 550 (1998)

28. B. J. Ramshaw *et. al.*, A quantum critical point at the heart of high temperature superconductivity. *Science* **348**, 317 (2015).

29. J. G. Analytis *et. al.*, Transport near a quantum critical point in $BaFe_2(As_{1x}P_x)_2$. *Nat. Phys.* **10**, 194197 (2014).

30. K. Fujita *et. al.*, Simultaneous Transitions in Cuprate Momentum-Space Topology and Electronic Symmetry Breaking. *Science* **344**, 612 (2014).

31. Max A. Metlitski, David F. Mross, Subir Sachdev, T. Senthil, Cooper pairing in non-Fermi liquids *Phys. Rev. B* **91**, 115111 (2015)

32. S. Lederer, Y. Schattner, E. Berg, S. A. Kivelson, Enhancement of superconductivity near a nematic quantum critical point. *Phys. Rev. Lett.* **114**, 097001 (2015)

33. T.A. Maier, D.J. Scalapino, Pairing interaction near a nematic QCP of a 3-band CuO_2 model. arXiv:1405.5238 (unpublished).

34. There are several different ways to define a nematic order parameter in terms of equilibrium electronic correlation functions. Correspondingly, there is an ambiguity in defining the nematic susceptibility. Thus the constants c and c' not only depend on microscopic details, but they also depend on the precise microscopic definition we give to the nematic order parameter.

35. Typical strains using this method are of order $10^{-3} \sim 10^{-4}$.

36. See supplementary material.

37. A. Tamai *et. al.*, Strong Electron Correlations in the Normal State of the Iron-Based $FeSe_{0.42}Te_{0.58}$ Superconductor Observed by Angle-Resolved Photoemission Spectroscopy *Phys. Rev. Lett.* **104**, 097002 (2010)

38. Alexandre Pourret *et. al.*,Strong correlation and low carrier density in $Fe_{1+y}Te_{0.6}Se_{0.4}$ as seen from its thermoelectric response *Phys. Rev. B* **83**, 020504(R) (2011)

39. A. Liam Fitzpatrick, S. Kachru, J. Kaplan, S. Raghu, Non-Fermi-liquid fixed point in a Wilsonian theory of quantum critical metals. *Phys. Rev. B* **88**, 125116 (2013).

40. Sean A. Hartnoll, Raghu Mahajan, Matthias Punk, Subir Sachdev, Transport near the Ising-nematic quantum critical point of metals in two dimensions. *Phys. Rev. B* **89**, 155130 (2014)

41. Preliminary confirmation that the nematic susceptibility at criticality diverges as $1//T$ has been obtained from determinantal Monte Carlo calculations of a 2D metallic nematic quantum critical system. Y. Shatner, S. Lederer, S.A. Kivelson, E. Berg, arXiv:1511.03282

42. J.G. Analytis, J.-H. Chu, R.D. McDonald, S. C. Riggs, I.R. Fisher, Enhanced Fermi surface nesting in superconducting $BaFe_2(As_{1-x}P_x)_2$ revealed by the de Haas-van Alphen effect. *Phys. Rev. Lett.* **105**, 207004 (2010)

43. H. Shishido *et. al.*, Evolution of the Fermi Surface of $BaFe_2(As_{1x}P_x)_2$ on Entering the Superconducting Dome. *Phys. Rev. Lett.* **104**, 057008 (2010).

44. While most of the samples used in this paper are in the size range of full strain transmission, it is important to note that the phosphorus substituted iron arsenide samples are $\sim 300\mu$m square and are in the regime of smaller strain transmission.

45. M. C. Shapiro, Patrik Hlobil, A. T. Hristov, Akash V. Maharaj, I. R. Fisher. Symmetry constraints on the elastoresistivity tensor. arXiv:1509.05462 [cond-mat.str-el]

46. Part No. PSt 150/557, from Piezomechanik, Munich, Germany.

47. J.-H. Chu, J. G. Analytis, C. Kucharczyk, I. R. Fisher, Determination of the phase diagram of the electron doped superconductor $Ba(Fe_{1-x}Co_x)_2As_2$. *Phys. Rev. B* **79**, 014506 (2009).

48. H. C. Montgomery, Method for Measuring Electrical Rsistivity of Anisotropic Materials. *Journal of Applied Physics* **42**, 2971 (1971); doi: 10.1063/1.1660656.

49. C.A. M. does Santos, A. de Campos, M. S. da Luz, B. D. White, J. J. Neumeier, B. S. de Lima, C. Y. Shigue, Procedure for measuring electrical resistivity of anisotropic materials: A revision of the Montogmery method. *Journal of Applied Physics* **110**, 083703 (2011); doi: 10.1063/1.3652905.

50. Part No. WK-XX-062TT-350, General Purpose Strain Gages - Tee Rosette, from Vishay Precision Group.

51. Y. Sun, S. Thompson, T. Nishida, *Strain effect in semiconductors: Theory and Device Applications* (Springer, New York, 2010).

52. Part No. 14250, General Purpose Adhesive Epoxy, from Devcon, U.S.A.

53. D. Butkovicova *et al.*, Critical role of the sample preparation in experiments using piezoelectric actuators inducing uniaxial or biaxial strains. *Rev. Sci. Instr.* **84**, 103902 (2013).

54. H.-H. Kuo *et al.*, Possible origin of the nonmonotonic doping dependence of the in-plane resistivity anisotropy of $Ba(Fe_{1-x}T_x)_2As_2$ (T=Co, Ni and Cu). *Phys. Rev. B* **84**, 054540 (2011).

55. H-.H. Kuo *et al.*, Magneto-elastically coupled structural, magnetic and superconducting order parameters in $BaFe_2(As_{1-x}P_x)_2$. *Phys. Rev. B* **86**, 134507 (2012).

56. E. C. Blomberg *et. al.*, Sign-reversal of the in-plane resistivity anisotropy in hole-doped iron pnictides. *Nat. Comm.* **4**, 1914 (2013).

57. Maria N. Gastiasoro, I. Paul, Y. Wang, P.J. Hirschfeld, Brian M. Andersen, Emergent Defect States as a Source of Resistivity Anisotropy in the Nematic Phase of Iron Pnictides. *Phys. Rev. Lett.* **113**, 127001 (2014).

58. Wei Bao *et. al.*, Tunable ($\delta\pi$, $\delta\pi$)-Type Antiferromagnetic Order in α-Fe(Te,Se) Superconductors. *Phys. Rev. Lett.* **102**, 247001 (2009).

59. T. M. McQueen, *et. al.*, Tetragonal-to-Orthorhombic Structural Phase Transition at 90 K in the Superconductor $Fe_{1.01}Se$ *Phys. Rev. Lett.* **103**, 057002 (2009).

60. D. S. Fisher, Random transverse field Ising spin chains. *Phys. Rev. Lett.* **69**, 534 (1992).

61. Olexei Motrunich, Siun-Chuon Mau, David A. Huse, Daniel S. Fisher, Infinite-randomness quantum Ising critical fixed points. *Phys. Rev. B* **61**, 1160 (2000).

62. E. W. Carlson, K. A. Dahmen, Using disorder to detect locally ordered electron nematics via hysteresis. *Nat. Comm.* **2**, 379 (2011).

Acknowledgments

This is the author's version of the work. It is posted here by permission of the AAAS for personal use, not for redistribution. The definitive version was published in Science Journal, Ubiquitous signatures of nematic quantum criticality in optimally doped Fe-based superconductors, Vol. 352, (20 May 2016), doi: 10.1126/science.aab0103 (`http://science.sciencemag.org/content/352/6288/958.full`).

The authors thank S. Raghu, S. Lederer, E. M. Spanton for helpful discussions. Johanna Palmstrom is supported by a Gabilan Stanford Graduate Fellowship and a National Science Foundation Graduate Research Fellowship. This work was supported by the DOE, Office of Basic Energy Sciences, under Contract No. DE-AC02-76SF00515 and by the National Science Foundation Graduate Research Fellowship under Grant No. DGE-114747.

Supplementary Materials

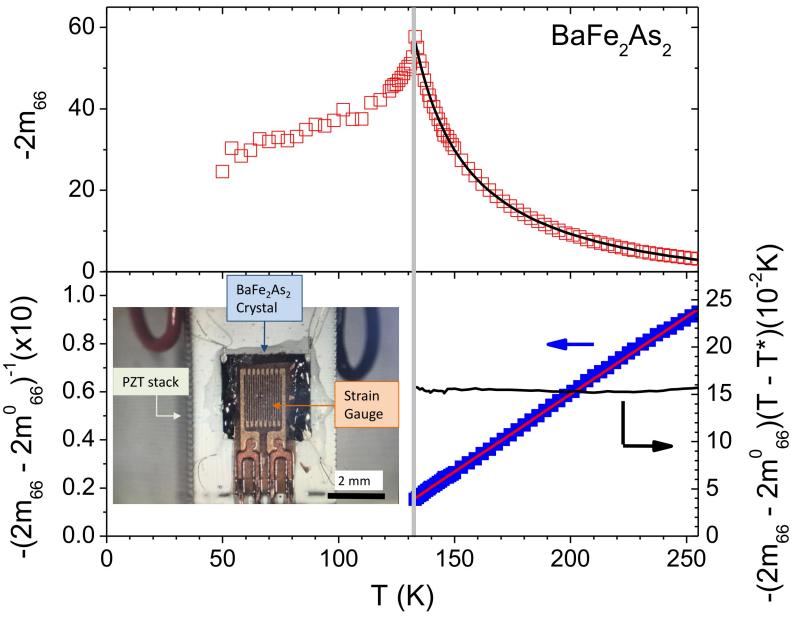

Figure 1: **Temperature dependence of the B_{2g} elastoresistance of $BaFe_2As_2$.** The data follow a Curie-Weiss behavior, which is the anticipated mean-field temperature dependence of the nematic susceptibility of a material approaching a thermally driven nematic phase transition (*13, 14, 15*). Upper panel shows $-2m_{66}$, proportional to the nematic susceptibility $\chi_{N(B_{2g})}$. Black line shows the Curie-Weiss fit. The quality of fit can be better appreciated by considering the inverse susceptibility, $-(2m_{66} - 2m_{66}^0)^{-1}$ which is perfectly linear (left axis of lower panel; fit shown by red line), and the Curie constant $-(2m_{66} - 2m_{66}^0)^{-1}(T - T^*)$ (right axis of lower panel), which is independent of temperature. The Weiss temperature obtained from the Curie-Weiss fit, which gives the bare mean field nematic critical temperature, yields a value T^* = 109 $\pm$1.4 K. Coupling to the lattice renormalizes the critical temperature, leading to a nematic-structural phase transition at T_s = 134 K (vertical gray line). Inset shows a photograph of a square crystal glued on a PZT piezoelectric stack for differential elastoresistance measurements using Montgomery's geometry. Four electrical contacts were made at the corners and a strain gauge was glued on the top surface (*36*).

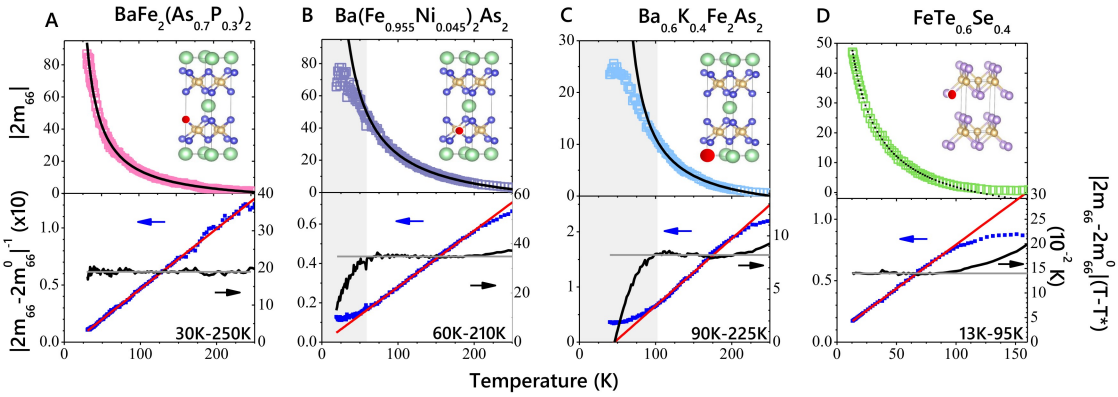

Figure 2: **Divergence of the B_{2g} elastoresistance $2m_{66}$ of several different families of optimally doped Fe pnictide and chalcogenide superconductors.** (A) optimally doped $BaFe_2(As_{0.7}P_{0.3})_2$ (isovalent substitution), (B) optimally doped $Ba(Fe_{0.955}Ni_{0.045})_2As_2$ (electron doped), (C) optimally doped $Ba_{0.58}K_{0.42}Fe_2As_2$ (hole doped), and (D) optimally doped $FeTe_{0.58}Se_{0.42}$. Insets indicate the dopant site (red) in the respective unit cells of each material. Comparable magnitude induced resistivity anisotropies are observed for each case (*36*). Upper panels show $|2m_{66}|$, whereas lower panels show $|(2m_{66} - 2m_{66}^0)|^{-1}$ (left axes of lower panels, blue symbols) and $|(2m_{66} - 2m_{66}^0)|(T - T^*)$ (right axes of lower panels, black curves). Black(upper panels) and red(low panels) lines shows fits to Curie-Weiss behavior of m_{66} and $|(2m_{66} - 2m_{66}^0)|^{-1}$ respectively. Grey horizontal lines (low panels) shows the average values of $|(2m_{66} - 2m_{66}^0)|(T - T^*)$ in the fitting temperature range. Regions of deviation from Curie-Weiss behavior in (B) and (C) are indicated by gray shaded regions. For (A) and (B), $2m_{66}$ is negative. For (C) and (D), $2m_{66}$ is positive. Fit parameters are listed in (*36, 44*).

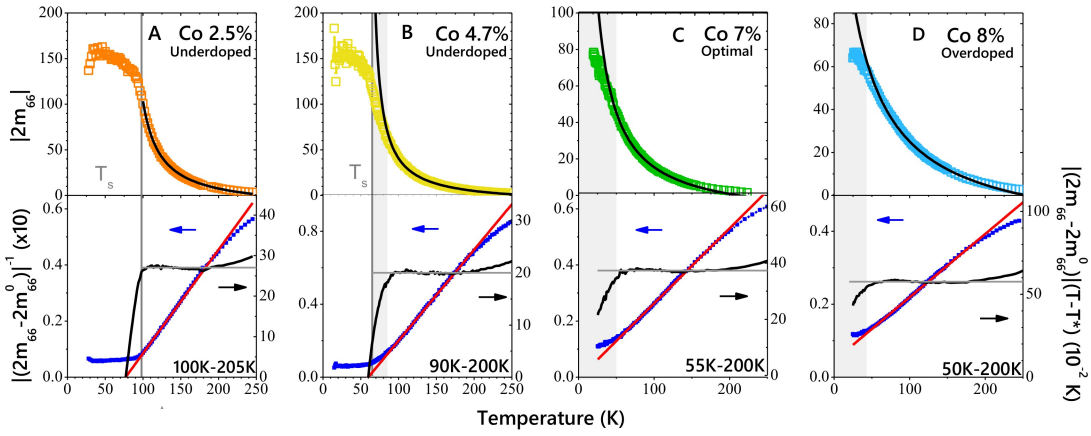

Figure 3: **Variation of the B_{2g} elastoresistance of Ba(Fe$_{1-x}$Co$_x$)$_2$As$_2$ for four representative compositions.** (A,B) underdoped compositions Ba(Fe$_{0.975}$Co$_{0.025}$)$_2$As$_2$ and Ba(Fe$_{0.953}$Co$_{0.047}$)$_2$As$_2$; (C) optimal-doped Ba(Fe$_{0.93}$Co$_{0.07}$)$_2$As$_2$; and (D) overdoped Ba(Fe$_{0.92}$Co$_{0.08}$)$_2$As$_2$. The heavily underdoped composition is very well described by a Curie-Weiss temperature dependence over the entire temperature range(black lines in upper panels). For the compositions near optimally-doping, $2m_{66}$ can be well fit by a Curie-Weiss T-dependence at high temperatures. Below a characteristic temperature scale(different for each compositions, indicated by shade gray region), a strong downward deviation from Curie Weiss behavior is observed, also seen in the inverse susceptibility (upward curvature) and in $|(2m_{66} - 2m_{66}^0)|(T - T^*) \propto \chi_N(T - T^*)$ (strong downturn), which are shown in the lower panels. The deviation from Curie-Weiss behavior is the strongest at the optimal doping, and diminishes on either side of the phase diagram. Curie-Weiss fit parameters for each composition are listed in (*36*).

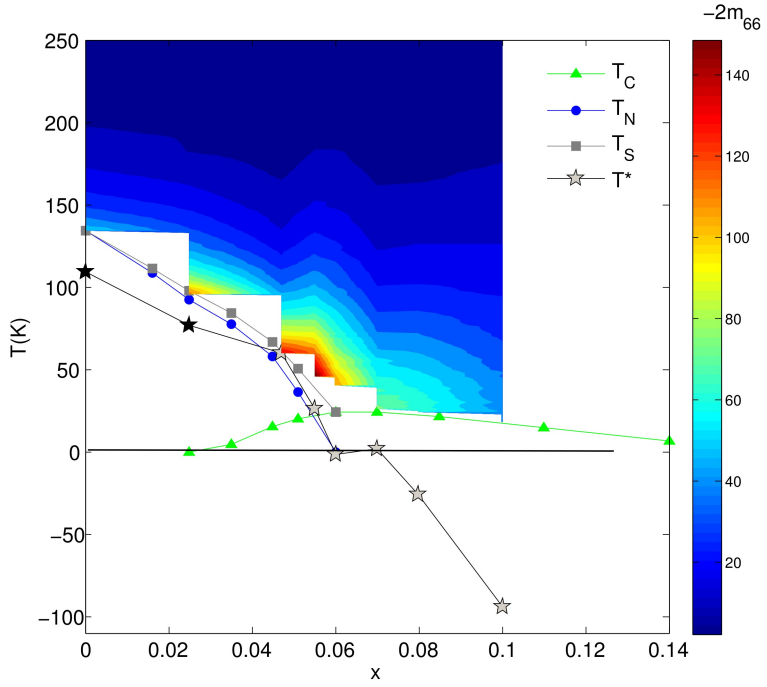

Figure 4: **Phase diagram of Ba(Fe$_{1-x}$Co$_x$)$_2$As$_2$, showing the variation of $2m_{66}$ in the $x-T$ plane (color scale).** Squares, circles and triangles indicate T$_s$, T$_N$, and T$_c$ respectively. Stars indicate the bare mean-field nematic critical temperatures, T^*, extracted from the Curie-Weiss fits of $2m_{66}$ above the temperature at which disorder effects suppress the nematic susceptibility (see text; light grey symbols are used for the cases for which deviations from Curie Weiss behavior are observed at low temperatures). As has been previously determined via longitudinal elastoresistance measurements (*13*), but established here by the full B_{2g} differential elastoresistance, the Weiss temperature, T^* goes through zero as a function of x close to optimal doping. Color scale shows the magnitude of $-2m_{66}$, which peaks between lightly underdoped to optimal doped compositions.